Inclusive pion double charge exchange on ^{16}O at 0.6 − 1.1 GeV

B.M. Abramov, Yu.A. Borodin, S.A. Bulychjov, I.A. Dukhovskoy, A.B. Kaidalov, A.P. Krutenkova, V.V. Kulikov, M.A. Matsyuk, I.A. Radkevich [1], E.N. Turdakina

State Research Center – Institute for Theoretical and Experimental Physics, 117218 Moscow, Russian Federation

L. Alvarez-Ruso

Nuclear Science Division, Lawrence Berkeley National Laboratory 1 Cyclotron Rd., Berkeley, CA 94720, USA

M.J. Vicente Vacas

Departamento de Física Teórica and IFIC, Centro Mixto Univesidad de Valencia-CSIC, Ap. Correos 22085, 46071 Valencia, Spain

Abstract

The inclusive pion double charge exchange (DCX) on oxygen nuclei has been measured in the region where additional pion production is kinematically forbidden. The experiment was performed at the ITEP PS at incident π^- kinetic energies $T_0 = 0.59$, 0.75 and 1.1 GeV. The integrated forward differential cross section was found to decrease with energy slowly. At 1.1 GeV it exceeds the theoretical prediction within the conventional sequential single charge exchange mechanism with a neutral pion in the intermediate state (Glauber elastic rescattering) by about a factor of five. The sequential mechanism with two pions in the intermediate state (Glauber inelastic rescatterings), which was proposed recently, seems to be able to explain the observed energy dependence and allows to predict the DCX cross section at higher energies.

Key words: pion double charge exchange, sequential single charge exchange mechanism, inelastic Glauber rescatterings

[1] Deceased

1 Introduction

Although pion double charge exchange (DCX) reactions on nuclei have long been studied, understanding the reaction mechanism within models of pion propagation through a nucleus appears to be a complicated problem because of the two-nucleon nature of the process. Nevertheless the unique feature of pion DCX of requiring at least two like nucleons of a nucleus to participate provides a good testing ground for an investigation of different few-body and nuclear structure effects in the nucleus (see [1]-[3] and references therein). The pion DCX process was first suggested as a probe of short range nucleon-nucleon correlations by De Shalit, Drell and Lipkin in 1961 [4]. The pioneering measurement of pion DCX was done at JINR [5] in 1963 at 30 – 80 MeV in inclusive reactions. The next step was made at meson factories which gave start to the investigation of exclusive DCX reactions since 1977. While these reactions were mainly used for the study of nuclear structure effects (excitation of double isobar-analog transitions, search for exotic nuclear states etc.), both inclusive and exclusive DCX measurements are important to study hadron dynamics.

For energies up to 0.5 GeV the conventional mechanism of two sequential single charge exchanges (SSCX) has traditionally been able to explain the main features of pion DCX. The thorough experimental investigations of the differential cross sections of inclusive DCX reactions, $A(\pi^{\pm},\pi^{\mp})\mathrm{X}$, for a wide range of nuclei from ^{3}He to ^{208}Pb in the energy region of Δ resonance (see Ref. [6]-[8] and the recent theoretical analysis [9]) confirmed that the SSCX is the dominant mechanism. The rather smooth energy dependence of forward exclusive DCX cross section from 0.3 to 0.5 GeV [3], [10] was successfully reproduced by Oset et al. in [11] within SSCX calculations in the Glauber approach using known $\pi\mathrm{N}$ amplitudes. For higher energies these authors [11] predicted a strong decrease of forward exclusive DCX cross section. Any significant deviation from the expected low value of the DCX cross section near 1 GeV offers a unique possibility to search for nonconventional DCX mechanisms (short range NN correlations, in particular) [11], [12].

We present here an experimental study of inclusive pion DCX at energies above 0.5 GeV, where there are no data available. Inclusive processes have much larger cross sections than exclusive ones and their registration does not require an excellent energy resolution. So, they are within existing experimental possibilities. Theoretically, the energy behaviour of the inclusive reactions seems less sensitive to the details of the nuclear structure and within the SSCX model reflects the energy dependence of the $\pi\mathrm{N}$ single charge exchange (SCX) amplitude [13]. At high energy, the DCX reactions can be studied in the kinematical region near the high-energy end point of the pion spectra, where pion production (the $(\pi,\pi\pi)$ process) on one nucleon is kinematically forbidden. The few existing experiments on DCX at high energies [14,15] have no events in this specific region of true DCX. For example, the events measured at $T_{\pi}=1.7$ GeV on ^{4}He [15] belong to the region where both

true DCX and two-pion production on a single nucleon coexist. Actually, the analysis performed in Ref. [15] reveals the dominance of the later mechanism followed by a two-body pion absorption at this energy.

The goal of this study is to get an information to clarify the mechanism of pion DCX on nuclei in the energy region near 1 GeV. Our preliminary results [16] and [17], obtained at the ITEP PS definitely showed that at 0.75 GeV and at 1.1 GeV we observed a pion DCX signal at a higher level than predicted in the framework of the SSCX model. The attempts [18] and [19] to explain this observation have led to the suggestion of a new mechanism [19] of pion DCX at energies above 0.6 GeV.

The results considered below are based on our full statistics of π^+ energy spectra from the reaction

$$\pi^- + {}^{16}\mathrm{O} \rightarrow \pi^+ + \mathrm{X} \tag{1}$$

at $T_0 = 0.59$, 0.75 and 1.1 GeV (scattering angle $\theta = 0 - 14^o$).

The paper is organized as follows. The experimental setup and data taking procedure are described in Section 2. Event selection is presented in Section 3. The DCX cross section calculation and an analysis of our results on π^+ spectra are given in Section 4. In Section 5 the comparison of the experimental data with the SSCX model is made. Energy dependence of DCX cross section is discussed in Section 6. Nonconventional mechanisms of DCX and the theoretical interpretation of the results are discussed in Section 7. Conclusion is given in Section 8.

2 Experimental setup and data taking

The data were taken at the ITEP 10-GeV Proton Synchrotron using negative pion beams with momenta $p_0 = 0.72$, 0.88 and 1.26 GeV/c ($T_0 = 0.59$, 0.75 and 1.1 GeV). [1] The beam flux was (1 - 5) $\times 10^5$ pions per 1 second spill. The experiment was done at the 3m magnet spectrometer instrumented with multigap optical spark chambers [20]. The layout of the experimental setup is shown in Fig. 1. The beam pions, defined by scintillation hodoscope H_1 and scintillation counters C_2 and C_3, struck the target placed in the middle of the magnet. The hodoscope H_1 (of 24 scintillation counters placed at the intermediate focus of the beam) made it possible to determine a beam pion momentum with a precision of $\pm$0.3%, while the full momentum acceptance of the beam was $\Delta p/p \sim$5%. The scintillation counter C_6 was used only for the beam adjustment. During the runs, the proportional chambers PC_1 and PC_2 served for the on-line monitoring of the beam position at the entrance of the target. Most of the beam particles passing through the target without interaction

[1] The values of p_0 and T_0 are related to the middle of the target.

were vetoed by the counter C_5. Čerenkov counter $\check{C}_2$ filled with freon-12 was used to reject electrons. The electron contamination in the beam was 10%, 6.5% and 3% at $p_0 = 0.72$, 0.88 and 1.26 GeV/c, respectively. Beam particle trajectories were reconstructed with the help of the beam spark chamber (BSC, 10 gaps, 1 gap = 0.8 cm) and large spark chambers (LSC 1 - 3, 32 gaps in total) placed in the magnetic field.

The H_2O and D_2O targets were contained in the identical cylindrical cells (with 8 cm in diameter and 9.5 cm in length) made of 0.014 cm stainless steel. They were positioned on the turnplate together with ^{6}Li, ^{7}Li, ^{12}C and "empty" targets. During each run they were substituted one for another at regular time intervals. The preliminary results with ^{6}Li and ^{7}Li targets can be found in [16] and [21]. The results for ^{12}C will be published elsewhere.

Positive particles from the reactions

$$\pi^- + A \rightarrow (\mathrm{e}^+, \pi^+, \mathrm{p}, \mathrm{d}) + \mathrm{X}, \tag{2}$$

emitted from the target in the forward direction were detected in three planes of scintillation hodoscopes H_5, H_2 and H_3 (14 elements with overall area $\sim$1.5 m^2). A time-of-flight (TOF) between C_2 and H_3 (on the base of $\sim$6 m) was measured to select pions, protons and deuterons with the appropriate triggers [2] . The outgoing particle momentum was measured in the large spark chambers LSC 4 - 6 (30 gaps in total), placed in the magnet. For each beam momentum the current in the magnet was set proportional to the beam momentum to have the same space topology of the events in the spectrometer. Pions were discriminated from protons/deuterons using the TOF measurement and from positrons using signals from the high pressure threshold Čerenkov counter $\check{C}_3$ [24] of 1.6 m in diameter filled with freon-12.

Sparks, coded hodoscope hits and a TOF code (and some other information) were photographed by a fast camera. All pictures without preliminary scanning were measured by a flying-spot digitizer PSP-2. Spark positions were reconstructed in space and the track parameters were calculated. Event recognition, reconstruction and DST (data summary tape) production were carried out with the set of computer codes developed for our spectrometer [25]. For each event the information written to the DST included the momenta of incoming and outgoing particles at the vertex, vertex coordinates, hodoscope hits, TOF values, etc. The analysis of the DST was carried out with the help of the HBOOK package.

[2] The proton and the deuteron triggers used the scintillation hodoscope H_4 and the scintillation counter C_7 in coincidence to detect backward π^-. With these triggers backward quasielastic π^-p and π^-d scattering was studied. The preliminary results were published in [22] and in [23], respectively.

About 37000 pictures were taken with the H_2O and D_2O targets with pion triggers

$$S_\pi = (H_1 C_2 C_3 \bar{\breve{C}}_2)\bar{C}_5(H_5 H_2 H_3 \bar{\breve{C}}_3)(C_2 H_3)_{t\pi}, \tag{3}$$

where Čerenkov counters $\breve{C}_2$ and $\breve{C}_3$ were used to reject electrons /positrons, and

$$S'_\pi = (H_1 C_2 C_3)\bar{C}_5(H_5 H_2 H_3)(C_2 H_3)_{t\pi}; \tag{4}$$

both triggers selected pions by the TOF coincidence window $(C_2H_3)_{t\pi}$. These triggers worked simultaneously with the proton and the deuteron triggers (see footnote 2). With the S_π trigger not only the cross section of the reaction (1) was measured but also the positron background (using the tagged $\breve{C}_3$ signal). The measured positron background allowed to extract the cross section of the reaction (1) also from the events of the S'_π trigger. However Čerenkov counters limited the acceptance of the setup for the proton and the deuteron triggers. So, a part of the statistics was taken with the S_π trigger and another part with the S'_π trigger.

The numbers of events, $N_{\rm DST}$, written to the DST with the S_π trigger were 22060, 2456 and 1752 at T_0 = 0.59 , 0.75 and 1.1 GeV, respectively, and with the S'_π trigger were 5395 and 5073 at T_0 = 0.75 and 1.1 GeV.

3 $\pi^-\,{}^{16}\mathrm{O} \to \pi^+\,\mathrm{X}$ event selection

Events of the reaction (1), which has relatively low cross section, constituted a small part of $N_{\rm DST}$, the main part came from the beam scattering off the magnet coil and yoke. The contribution of these events, as well as of those originating from the outgoing particle interaction in the material of hodoscopes H_5, H_2 and H_3, was effectively suppressed by two requirements: the trajectory of forward going particle should be successfully reconstructed in all three spark chambers LSC 4 - 6, and the extrapolated trajectory should cross the hit elements of the hodoscopes. The final sample contained the events of the reaction (1), proton background from the reaction (2) and also positron background (only for the S'_π trigger).

The proton background was mainly suppressed by the TOF coincidence $(C_2H_3)_{t\pi}$ on the trigger level. The typical distribution of M_t^2, the outgoing particle mass squared [3], is shown in Fig. 2 for a sum of pion (S_π), proton and deuteron triggers taken at $T_0 = 0.59$ GeV. The hatched area in Fig. 2 shows the events of the pion

[3] M_t was calculated using the relation $M_t^2 = p^2(1-\beta^2)/\beta^2$, where p is a particle momentum measured by the spectrometer and β is the velocity determined by the TOF measurement ($1/\beta = \alpha(N - N_0)$, where N is the TDC channel number and α and N_0 are known constants).

trigger, which accepted also protons with relatively high momenta. In the momentum distribution of these events (see Fig. 3) the two groups of events within the momentum acceptance of the apparatus (solid curve) are protons (at higher momenta) and pions. The cut on M_t^2 (events between the arrows in Fig. 2) practically suppressed the events to the right of the beam momentum (protons) (see hatched histogram in Fig. 3). The remaining events in this region were considered as the proton background from the non Gaussian TOF tail.

The DCX candidates for the reaction (1) lie at the high-energy part of the pion spectrum in the kinematical region $\Delta T = T_0 - T \leq m_\pi \simeq 140$ MeV (T is the kinetic energy of outgoing pion), where the additional pion production is forbidden. The number of the DCX candidates was 434, 77 and 15 for T_0 = 0.59, 0.75 and 1.1 GeV. The proton background in the DCX region was estimated by the extrapolation of the distribution with the momentum higher than p_0 to the lower momentum region (for T_0 = 0.59 GeV see hatched histogram in Fig. 3). The extrapolation function was taken from the momentum distribution of protons from the reaction π^-p$\rightarrow$pX measured separately. This function weakly decreased with the decrease of momentum. The contribution of the proton background events to the DCX region increased with the beam momentum and appeared to be (6 $\pm$ 1)%, (13 $\pm$ 4)% and (20 $\pm$ 9)% for T_0 = 0.59, 0.75 and 1.1 GeV in the S_π trigger. The positron background was rejected in this trigger with the use of Čerenkov counters.

In order to select the events of the reaction (1) in the S'_π trigger, it was necessary also to eliminate the beam positron background, BPB, and to subtract the target positron background, TPB. The BPB came from the electron admixture in the beam, which produced fast forward positrons via bremsstrahlung in the target (following by the γ conversion into $\mathrm{e}^+_{\mathrm{forward}}\mathrm{e}^-$ pair). Forward positrons gave a sharp peak in the beam direction while pions and protons had a flat distribution within the acceptance. In Fig. 4 we show the distributions of outgoing positive particles (pions, protons and positrons) on the vertical projection of the reaction angle, $\Delta\lambda$ (contrary to the horizontal one it was not distorted by the influence of the magnetic field). The hatched histogram in this figure stands for protons. The width of the zero-angle positron peak was determined by multiple scattering in the target ($\sigma_{\Delta\lambda} \lesssim 0.005$ rad for water target at $T_0 = 1.1$ GeV). The cut $|\Delta\lambda| \geq 0.03$ rad (see vertical arrows in Fig. 4) rejected the BPB in the S'_π trigger to a level of less than 3%.

The momentum distribution, analogous to the one presented in Fig. 3 for $T_0 = 0.59$ GeV and the S_π trigger is shown in Fig. 5 for $T_0 = 1.1$ GeV and the S'_π trigger events. Here, the additional cut $|\Delta\lambda| \geq 0.03$ rad was applied to reject BPB (for more details see [26]). The DCX region in this case contains events of the reaction (1) and of proton and positron (TPB) backgrounds. The number of the DCX candidates was 45 and 57 respectively for T_0 = 0.75 and 1.1 GeV. The contribution of the proton background events to the DCX region was (10 $\pm$ 5)% and (15 $\pm$ 7)% for T_0 = 0.75 and 1.1 GeV, respectively.

TPB is induced by the beam pion interaction in the target ($\pi^- A \to \pi^0 A'$, $\pi^0 \to \gamma\gamma, \gamma \to \mathrm{e}^+_{\mathrm{forward}}\mathrm{e}^-$ or from Dalitz decay $\pi^0 \to \mathrm{e}^+_{\mathrm{forward}}\mathrm{e}^-\gamma$). The use of Čerenkov detector $\check{C}_3$ with the S_π trigger suppressed this background, while in the S'_π trigger we should take it into account. To estimate TPB we analyzed the $\check{C}_3$ signal in the S_π trigger in order to select events with forward going positrons and pions. The $\check{C}_3$ signals due to knockout of δ electrons in $\check{C}_3$ and to the noise of its PMTs were also taken into account. The ratio of TPB events to the DCX candidates (pions plus TPB) for $|\Delta\lambda| \geq 0.03$ rad was (12 $\pm$ 4)% and (14 $\pm$ 8)% for T_0 = 0.75 and 1.1 GeV, respectively.

4 Cross section calculation

The events which satisfied the requirements of the previous Section were taken as candidates for the reaction (1). In order to facilitate the comparison of the data at different energies, we used event distributions on $\Delta T = T_0 - T$ ($\Delta T > 0$). The calibration of the ΔT scale was checked using the position of the backward elastic π^-p scattering peak in the reaction $\pi^-\mathrm{p} \to \mathrm{pX}$ ($\mathrm{M}^2_{\mathrm{X}} = \mathrm{m}^2_\pi \simeq 0.0195$ GeV^2) for the proton trigger on the water target. The ΔT resolution was estimated from the width of this peak, and varied from 6 to 8 MeV for T_0 from 0.59 to 1.1 GeV. As an example, in Fig. 6 the proton spectrum obtained at T_0 = 0.59 GeV was fitted with a sum of two Gaussians (solid curve), one for the proton peak and another for the oxygen background (dashed curve).

In Fig. 7 angular distributions of the DCX events taken with the S_π trigger at $T_0 =$ 0.59 GeV are shown in comparison with the Monte Carlo (MC) calculations normalized to the same number of events. The calculations were performed assuming that the DCX differential cross section does not depend on a laboratory angle of π^+ emission. It can be seen from Fig. 7 that within our angular acceptance and statistics this assumption is in a good agreement with the data for all intervals of π^+ momentum. It allows us to calculate the differential cross section as an average over the angular acceptance using the following expression

$$\frac{\mathrm{d}^2\sigma(T_0,\Delta T)}{\mathrm{d}\Omega \mathrm{d}T} = \frac{N_{DCX}(T_0,\Delta T)}{(\rho l/A) N_{\mathrm{Av}} N_0 \Delta T \Delta\Omega(T_0,\Delta T)} \frac{b}{k}, \tag{5}$$

where $N_{DCX}(T_0,\Delta T)$ is the number of DCX candidates in the interval ΔT = 20 MeV; A is the target mass number, ρ and l are the target density and thickness, N_{Av} is the Avogadro constant, and N_0 is the beam flux.

The correction factor b takes into account the proton and the positron backgrounds. In the case of the S_π trigger, b = 0.94$\pm$0.01, 0.87$\pm$0.04 and 0.80$\pm$0.09 at $T_0 =$ 0.59, 0.75 and 1.1 GeV, respectively. For the S'_π trigger we have 0.71$\pm$0.06 and 0.71$\pm$0.09 at $T_0 =$ 0.75 and 1.1 GeV.

The correction parameter $k = \prod_i k_i,\ i = 1, 2, ..., 5$ accounts for lepton contamination in the beam (k_1), beam halo on the target (k_2), pion decay in the apparatus (k_3), pion absorption in the water target (k_4), and pion absorption in the detector material (k_5). Depending on the beam momentum the value of k varied from 0.53 to 0.75 with the uncertainty $\pm$ 0.04; k_1 = 0.81 – 0.94 ($\pm$ 0.02), k_2 = 0.77 – 0.96 ($\pm$ 0.04), k_3 = 0.94 – 0.97 ($\pm$ 0.03), k_4 = 0.87 – 0.92 ($\pm$ 0.02), and k_5 = 0.94 – 0.98 ($\pm$ 0.02). The empty-target background was measured during each run and varied within $3 \pm 1\ \%$. To check the overall cross section normalization we applied a procedure analogous to formula (5) to obtain the cross section of the backward elastic π^-p scattering with the proton trigger on a water target. The angular dependence of this cross section is in an agreement with the partial-wave analysis (PWA) of SAID [27] shown in Fig. 8 (solid line is the FA02 solution).

The forward differential cross section of the reaction (1) at the beam kinetic energies $T_0 = 0.59$, 0.75 and 1.1 GeV was calculated according to formula (5) as the mean value of the cross sections on H_2O and D_2O targets. The angular acceptance was θ = 0 – 14^o for the S_π trigger and 2 – 10^o for the S'_π trigger with the mean value $\approx$5^o. At T_0 = 0.59 GeV and with the S_π trigger, the spectra were measured for two settings of the hodoscope H_2, target and magnetic field, which provided small [17] and large ΔT acceptance with approximately the same mean accepted angle. In Fig. 9(a) the ΔT distribution obtained for the DCX cross section with the large acceptance is shown. The cross section grows monotonously in the range of ΔT from 0.03 to 0.25 GeV and has no peculiarity at the threshold of the additional pion production process. Within our resolution we don't see a signal of the ^{16}C ground state [28] from the reaction ^{16}O(π^-, π^+)^{16}C(g.s.), which could appear at ΔT =18.4 MeV.

In Figs. 9(b) and (c), we show the summed spectra obtained with the S_π and the S'_π triggers at 0.75 and 1.1 GeV. The cross sections integrated over the ΔT ranges from 0 to 80 MeV ($\langle$dσ/d$\Omega\rangle_{80}$)[4] and from 0 to 140 MeV ($\langle$dσ/d$\Omega\rangle_{140}$) with their statistical errors are presented in Table 1 for the S_π and the S'_π triggers separately. As their values are in a good agreement for each beam energy we calculated the average values of the integrated cross sections; they are placed in the last line of the Table 1. The systematic errors are $\approx 10\%$. The present values of $\langle$dσ/d$\Omega\rangle_{80}$ at 0.59 and 0.75 GeV are fully compatible with the preliminary results of Ref. [17].

5 Comparison with the SSCX model

The first step towards an interpretation of the experimental results is to compare them with a calculation based on the conventional SSCX mechanism, represented

[4] This ΔT interval was chosen to make the comparison with the inclusive data [29] at lower energy (LAMPF) which were kindly placed at our disposal by A.Williams.

Table 1
The DCX cross sections integrated over the ΔT range from 0 to 80 MeV, $\langle \mathrm{d}\sigma/\mathrm{d}\Omega \rangle_{80}$, and over the ΔT range from 0 to 140 MeV, $\langle \mathrm{d}\sigma/\mathrm{d}\Omega \rangle_{140}$, obtained using pion triggers S_π, and S'_π and the averaged values of these cross sections (last line).

	$\langle \mathrm{d}\sigma/\mathrm{d}\Omega \rangle_{80}$, $\mu b/sr$			$\langle \mathrm{d}\sigma/\mathrm{d}\Omega \rangle_{140}$, $\mu b/sr$		
T_0, GeV	0.59	0.75	1.1	0.59	0.75	1.1
S_π	18.8±2.1	11.6±2.3	11.4±4.0	80.2±4.3	43.4±5.1	23.3±6.5
S'_π		10.5±2.7	6.4±1.9		41.4±6.5	31.4±4.7
$\langle S_\pi + S'_\pi \rangle$	18.8±2.1	11.1±1.8	7.3±1.7	80.2±4.3	42.6±4.0	28.6±3.8

by diagram (a) in Fig. 10 ($H_0 = \pi^0$). For this purpose we have used a Monte-Carlo cascade model constructed to describe pion induced multichannel reactions (quasielastic, SCX, DCX, absorption and π production) at pion energies above 0.5 GeV [13]. This approach has been earlier applied to the description of pion-nucleus inclusive reactions (including DCX) at $T_\pi = 85 - 350$ MeV [30,31]. The basic idea is that a pion propagating inside a nucleus can undergo elastic or quasielastic collisions, be absorbed by two or three nucleons or produce another pion. The probabilities per unit length of these processes are included in the model, taking into account medium effects: Pauli blocking, Fermi motion and nucleon binding energy. Furthermore, the renormalization of the πN amplitude has been incorporated following Ref. [11]. When compared to the quasielastic data [13], the model was able to reproduce the quasielastic peak but underestimates pion production. This discrepancy is common to other cascade codes like, for example the cascade exciton model (CEM) [32] and has been addressed in a recent publication [33]. However, the present study, is mainly confined to the region where additional pion production is forbidden, and which is well described by SCX.

The SSCX contribution to the cross section of the reaction (1) calculated in the framework of the MC cascade model [13] is shown in Fig. 9 by the solid curves. Model predictions slightly overestimate the measured cross section for $\Delta T < 140$ MeV at T_0 = 0.59 GeV and strongly underestimate it at T_0 = 1.1 GeV. As for the pion production contribution, we can compare the theoretical predictions (see dashed curves in Fig. 9) with the experimental results only at T_0 = 0.59 GeV, where we have a large ΔT acceptance. It can be seen that the calculation overestimates the measured points. This discrepancy could be related to the fact that the pion production mechanism, the scattering angles and energies of the outgoing particles are assumed to follow the 3-body phase space distribution due to the lack of measured differential cross sections [13].

Since there are no other experimental data on the reaction (1) at our energies, we

performed calculations for the charge symmetric reaction

$$\pi^+ + {}^{16}\mathrm{O} \to \pi^- + \mathrm{X} \tag{6}$$

at $T_0 = 0.4$ – 0.5 GeV for $\theta = 5^o$ to compare them with the available data taken at LAMPF [29]. In Fig. 11 we see that the SSCX calculation (solid curve) overestimates these data. It is worth mentioning here, that the forward cross sections of the exclusive reactions ${}^{14}\mathrm{C}(\pi^+,\pi^-){}^{14}\mathrm{O}$ and ${}^{18}\mathrm{O}(\pi^+,\pi^-){}^{18}\mathrm{Ne}$, which were calculated within Glauber theory without free parameters [11], also appeared to be higher than the measured ones at $T_0 = 300$ – 525 MeV [10]. The authors of [11] succeeded in reaching an agreement with the data of [10] after they took into consideration a medium polarization, which led to the renormalization of the charge exchange $\pi\mathrm{N}$ amplitude. Taking this effect into account in our model substantially decreases the value of the DCX cross section for the reaction on ${}^{16}\mathrm{O}$ (see dashed curves in Fig. 11) and improves an agreement with the data at $T_0 = 0.59$ GeV. However for higher energies, as it will be shown in the next Section, it results in larger deviation from the data.

6 Energy dependence

In Fig. 12 and Fig. 13, the energy dependence of the partially integrated pion DCX cross sections $\langle \mathrm{d}\sigma/\mathrm{d}\Omega\rangle_{80}$ and $\langle \mathrm{d}\sigma/\mathrm{d}\Omega\rangle_{140}$ is shown. The results from the last line of Table 1 are presented by the black circles, while the experimental data of [7] for the reaction (1) at $T_0 = 0.18$, 0.21 and 0.24 GeV and $\theta = 25^o$, and the results of [29] on the reaction (6) are shown by empty circles and squares, respectively. The DCX cross section decreases with energy by about a factor of six from 0.18 to 1.1 GeV, but the cross section calculated within the SSCX model for $\theta = 5^o$ (solid curves in Fig. 12 and Fig. 13) falls considerably faster in the region of 0.6 – 1.1 GeV. This behaviour reflects the fast decrease of a single charge exchange $\pi\mathrm{N}$ amplitude in this energy region. At 0.75 and 1.1 GeV the measured cross section is significantly larger than expected from the conventional SSCX mechanism. Therefore, other (nonconventional) approaches to the high energy DCX or a substantial modification of $\pi\mathrm{N}$ amplitudes are needed to explain the observed discrepancy between theory and experiment.

The results of the theoretical calculations within the SSCX mechanism with medium polarization are shown by dashed-dotted curves marked with stars. The shape of these curves with and without medium polarization effect is similar and the discrepancy of the theory and the experiment gets even larger when it is taken into account.

Finally, let us note that the cross section of the exclusive reaction ${}^{16}\mathrm{O}(\pi^+,\pi^-){}^{16}\mathrm{Ne}$, that is a small part of the inclusive process (6), falls in the range 0.18 – 0.25 GeV

[34]-[35], then increases up to 0.3 GeV and stays constant within experimental errors up to 0.5 GeV [36].

7 Other approaches to pion DCX

We observed a large deviation of the measured DCX cross section from the SSCX prediction at high energy. Two new approaches have been tried to explain the phenomenon. The first calculations of the contribution of meson exchange currents (MEC) to DCX (see diagrams (c) in Fig. 10) in this energy region have been performed in [18] for the exclusive reaction $^{18}\mathrm{O}(\pi^+,\pi^-)^{18}\mathrm{Ne}$. At $T_0 > 0.5$ GeV they showed a weak energy dependence comparable with the one seen in our experiment for inclusive DCX. This reflects the very weak energy dependence of the MEC amplitudes. However, the absolute values of MEC amplitude appeared to be too small to be relevant.

A new idea was proposed in Ref. [19]. It was shown that the Glauber inelastic rescatterings (IR) (see diagram (a) in Fig. 10 with H^0 being a multipion state) gave an important contribution to the inclusive DCX cross section at energies $T_0 \gtrsim 0.6$ GeV and allowed to understand the relatively slow decrease of the cross section with energy. The cross section of the reaction (1) was expressed as the sum of two terms, one with an intermediate π^0 (SSCX) and another with an intermediate 2π state (IR contribution). The IR part was calculated [37] in the framework of the Gribov-Glauber approach to DCX using the experimental data on the reactions $\pi^-\mathrm{p} \to \pi\pi\mathrm{N}$ [38] and the one pion exchange (OPE) model (see diagram (b) in Fig. 10). The dotted and dashed curves in Figs. 12 and 13 correspond to upper and lower boundaries of the theoretical estimation. The upper limit is close to the experimental data, especially for $\langle \mathrm{d}\sigma/\mathrm{d}\Omega\rangle_{140}$, which represents a considerable improvement with respect to the SSCX calculation. Although at present the uncertainty in these predictions is rather large the IR contribution seems to be able to explain the observed energy dependence.

The analysis of [37] indicates that at higher energies the low-boundary curve (the dashed one) is more justified and that in this case the average distances, d, between nucleons participating in the interaction are relatively small: $d \sim (2m_{\mathrm{N}}\Delta T)^{-1/2}$. These nucleons are rather closely correlated and can be even considered as a 6-quark system corresponding to the diagram (d) in Fig. 10.

Although the diagrams (b) and the upper one in (c) (see Fig. 10), which stand for IR in the OPE model and MEC respectively, look similar, we would like to stress their principal difference: in the OPE model we treat the $\pi^-\pi^+$-scattering amplitude as a function of M^2 (M is the mass of the intermediate state H^0) and integrate it over this variable while in the MEC model the $\pi^-\pi^+$ amplitude is approximated as a point-like interaction taken at the threshold ($M = 2m_\pi$). Due to the soft pion

theorems the last amplitude is small and thus leads to small modifications of SSCX predictions [18]. We take into account both real and imaginary parts of $\pi^-\pi^+$ amplitude in the regions of M^2 where they are not small, so it is not surprising that our calculations for DCX cross sections are substantially higher than SSCX predictions (even for the dashed curves in Fig. 12 and Fig. 13).

8 Conclusion and outlook

In summary, we have performed the first measurement of the cross section for the forward inclusive reaction $\pi^- + ^{16}\mathrm{O} \to \pi^+ + \mathrm{X}$ at energies $T_0 = 0.59$ – 1.1 GeV, in the region where additional pion production is kinematically forbidden. We have found that the cross section decreases with energy considerably slower than it is predicted by the conventional DCX mechanism of two (or more) sequential single charge exchanges with a π^0 in the intermediate state. At $T_0 = 1.1$ GeV, the experimental cross section is a factor of five larger than the theoretical one. This discrepancy implies that new mechanisms should be invoked in the region of $T_0 \sim 1$ GeV. The contribution of two-pion intermediate states, obtained within the Glauber-Gribov framework, seems to play an important role but the large theoretical uncertainty of the calculation does not allow to come to more definite conclusion. Experimental data at higher energies will be extremely helpful to clarify the situation and to constrain this model.

Acknowledgements

We are grateful to the staff of the 3m spectrometer, of the ITEP PS as well as the PSP-2 group for the assistance during the experiment. We are pleased to thank G.A.Leksin for his interest to this study and for the discussions of the results. A.P.K. thanks I.S. and I.I.Tsukerman for permanent support. This work was supported in part by RFBR Grants 98-02-17179, 00-15-96545, 00-15-96786 and 01-02-17383, and by Grant INTAS-93-3455.

References

[1] R. P. Jibuti, and R. Ya.Kezerashvili, Fiz. Elem. Chastits Atom. Yadra, 16 (1985) 1173.

[2] H. Clement, Progr. Part. Nucl. Phys. 29 (1992) 175.

[3] M.B.Johnson, and C.L.Morris, Annual Rev. Nucl. Part. Sci. 43 (1993) 165.

[4] A. De Shalit, S. D. Drell, and H. Lipkin, Nuclear News, Weizmann Inst., Rehovot Dec., 1961.

[5] Yu. A. Batusov et al., Pis'ma Zh. Eksp. Teor. Fiz. 46 (1964) 817.

[6] P. A. M. Gram et al., Phys. Rev. Lett. 62 (1989) 1837.

[7] S.A. Wood et al., Phys. Rev. C46 (1992) 1903.

[8] M. Yuly et al., Phys. Rev. C55 (1997) 1848.

[9] M. Alqadi, and W. R. Gibbs, Phys. Rev. C65 (2002) 044609.

[10] A. Williams et al., Phys. Lett. B216 (1989) 11.

[11] E. Oset, and D. Strottman, Phys. Rev. Lett. 70 (1993) 146;

E. Oset, D. Strottman, H. Toki, and J. Navarro, Phys. Rev. C48 (1993) 2395.

[12] O. Hashimoto. "Future experimental projects with the superconducting kaon spectrometer". Preprint Tokyo Univ., INS-844, Sept. 1990; also in "Prespective of Meson Science" Ch. 19 (North Holland, Amsterdam-London-New York-Tokyo, 1992), p. 547.

[13] M.J. Vicente Vacas, M.Kh. Khankhasayev, and S.G. Mashnik, Preprint nucl-th/9412023.

[14] A. V. Arefyev et al. Proc. Intern. Symp."Interaction of high energy particles with nuclei", ITEP, Moscow, Sept. 1973, V. 2, p. 35 (in Russian).

[15] J.–B.Jeanneret, M.Bogdanski, and E.Jeannet, Nucl. Phys. A**350**, 345 (1980).

[16] B.M. Abramov et al., Few-Body Systems Suppl. 9 (1995) 237.

[17] B.M. Abramov et al., Yad. Fiz. 59 (1996) 399 (English translation: Phys. Atomic Nucl. 59 (1996) 376).

[18] L. Alvarez-Ruso, and M.J. Vicente Vacas, J. Phys. G: Nucl. Part. Phys. **22** (1996) L45.

[19] A.B. Kaidalov, and A.P. Krutenkova, Yad. Phys. 60 (1997) 1334
(English translation: Phys. Atomic Nucl. 60 (1997) 1206).

[20] B.M. Abramov et al., Nucl. Phys. A372 (1981) 301.

[21] B.M. Abramov et al.,Yad. Fiz. 65 (2002) 253 (English translation: Phys. Atomic Nucl. 65 (2002) 229).

[22] B.M. Abramov et al., Pis'ma Zh. Eksp. Teor. Fiz. 71 (2000) 524 (English translation: JETP Lett. 71 (2000) 359).

[23] B.M. Abramov et al., Pis'ma Zh. Eksp. Teor. Fiz. 74 (2001) 504 (English translation: JETP Lett. 74 (2001) 449).

[24] B.M. Abramov et al., Nucl. Instrum. Methods A248 (1986) 203.

[25] V.V. Kishkurno et al., Preprint ITEP 139, 1990 (in Russian).

[26] B.M. Abramov et al., Acta Physica Polonica 27B (1996) 3051.

[27] R.A. Arndt et al., Phys. Rev. C52 (1995) 2120.

[28] F. Ajzenberg-Selove, Nucl. Phys. A460 (1986) 1.

[29] R.G. Burleson, in *Pion–Nucleus Double Charge Exchange*, Proceedings of the Second LAMPF Workshop on Pion–Nucleus Double Charge Exchange, Los Alamos, New Mexico, USA, p.79. Singapore, World Scientific 1990.

[30] L.L. Salcedo, E. Oset, and M.J. Vicente Vacas, Nucl. Phys. A484 (1988) 557.

[31] M.J. Vicente Vacas, E. Oset, L.L. Salcedo, and C. García Recio, Phys. Rev. C39 (1989) 209.

[32] K.K. Gudima, S.G. Mashnik, and V.D. Toneev, Nucl. Phys. A401 (1983) 329.

[33] S.G. Mashnik, R.J. Peterson, A.J. Sierk, and M.R. Braunstein, Phys. Rev. C61 (2000) 034601.

[34] R. Gilman et al., Phys. Rev. C29 (1984) 2395.

[35] D.P. Beatty et al., Phys. Lett. B305 (1993) 13.

[36] D.P. Beatty et al., Phys. Rev. C48 (1993) 1428.

[37] A.B. Kaidalov, and A.P. Krutenkova, J. Phys. G: Nucl. Part. Phys. 27 (2001) 893.

[38] A.D. Brody et al. Phys. Rev. D4 (1971) 2693.

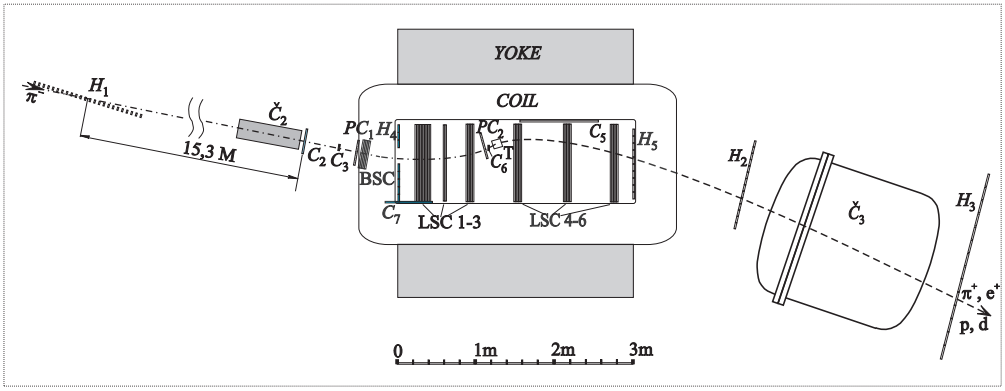

Fig. 1. The layout of the experimental setup.

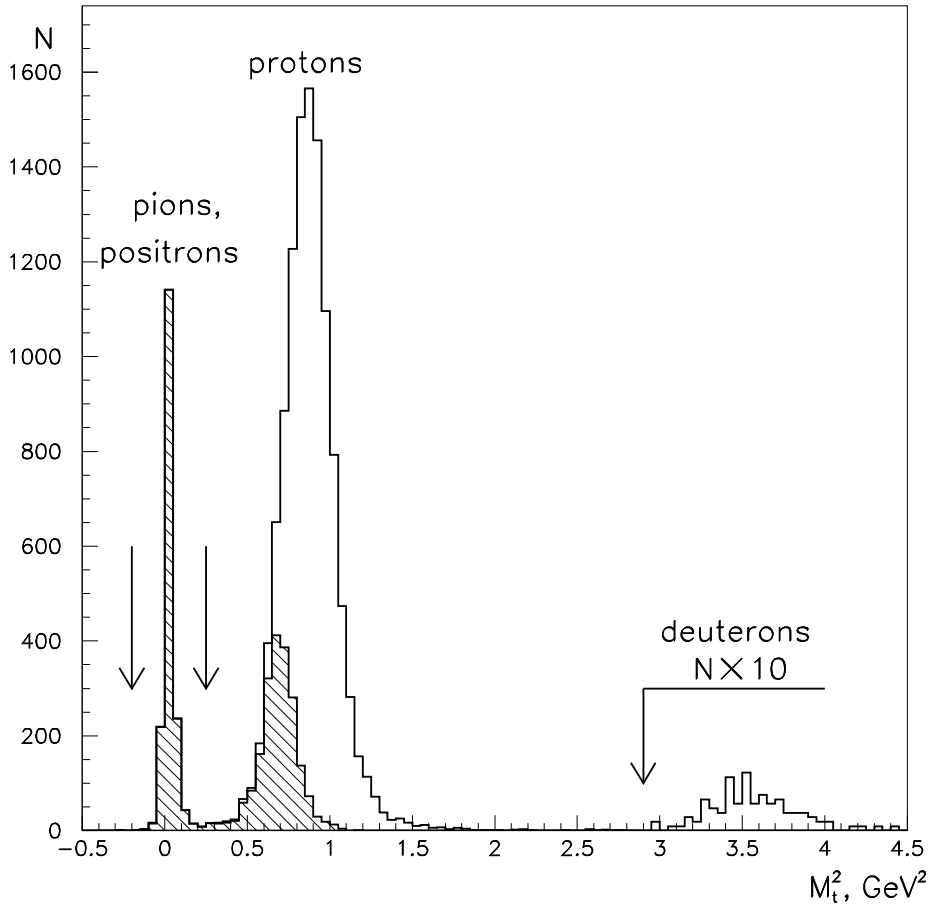

Fig. 2. The mass squared of positive particles from the reaction $\pi^- A \to (\mathrm{e}^+, \pi^+, \mathrm{p}, \mathrm{d})\mathrm{X}$, for the sum of events taken with a pion, a proton and a deuteron triggers at T_0 = 0.59 GeV. The hatched histogram corresponds to the pion (S_π) trigger.

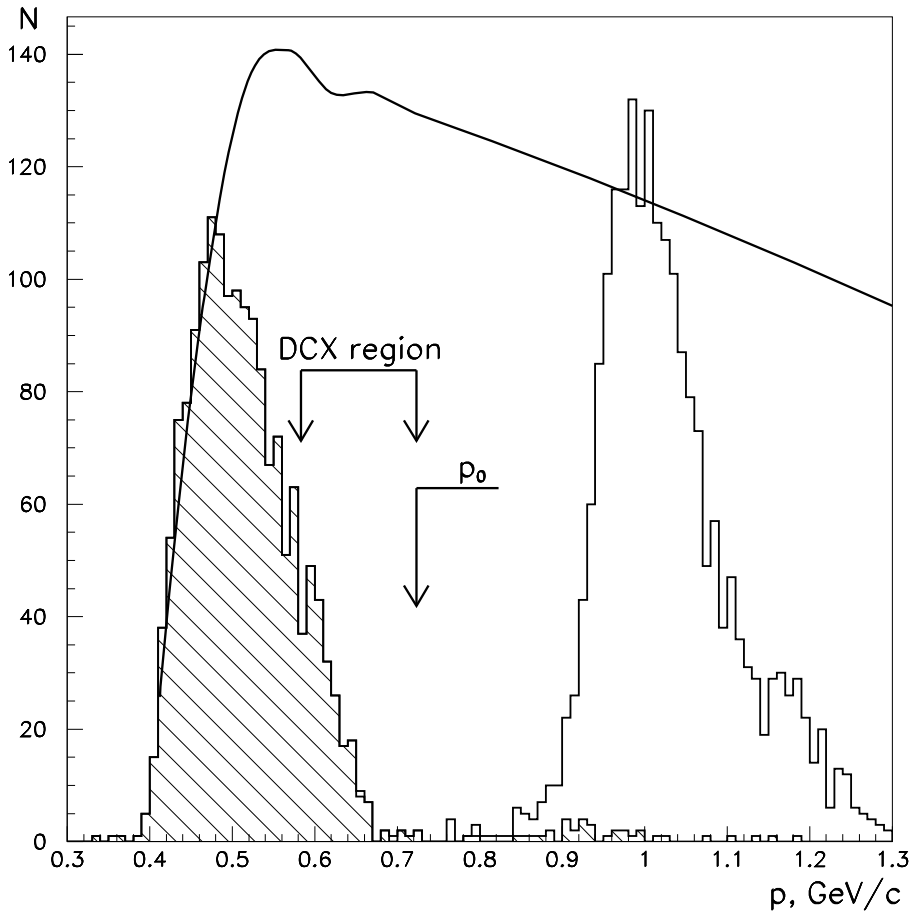

Fig. 3. The momentum distributions of the outgoing particle in the S_π trigger at T_0 = 0.59 GeV. The hatched histogram is after the cut on M_t^2 to reject protons. The solid curve is the acceptance of the apparatus (arbitrary units).

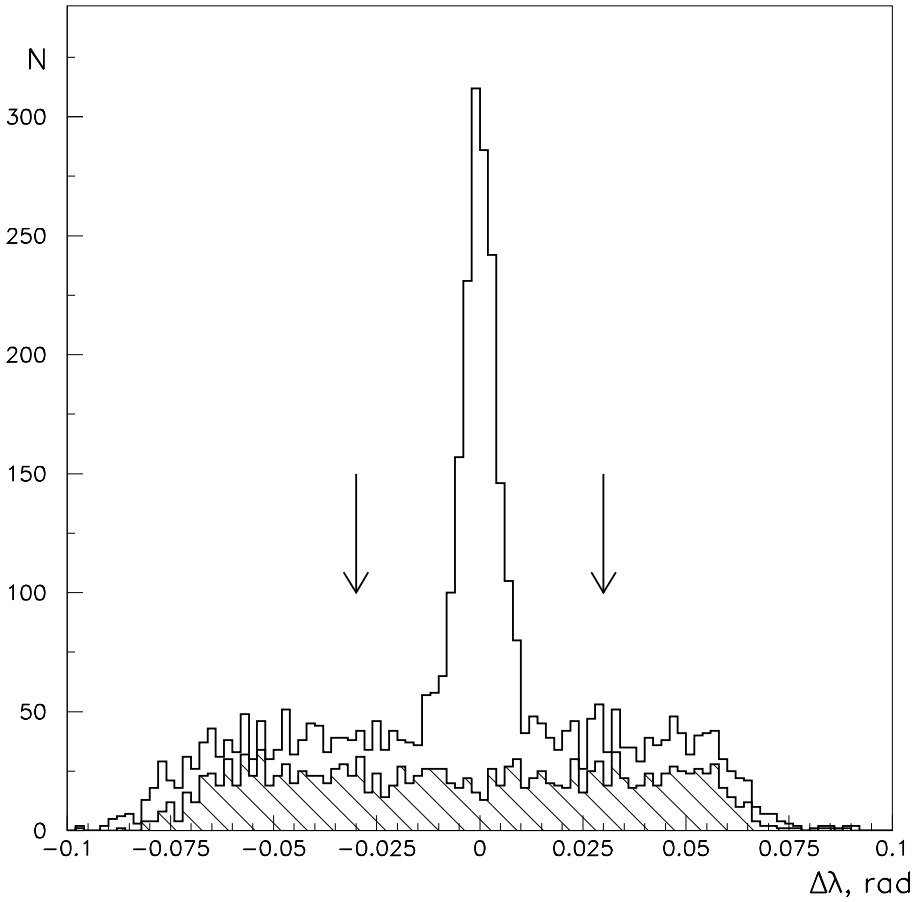

Fig. 4. The vertical projection of the reaction angle of the outgoing particles (e^+, π^+ and p) in the S'_π trigger. The hatched histogram is for the protons. Vertical arrows correspond to the $\Delta\lambda$ value of $\pm$ 0.03 rad.

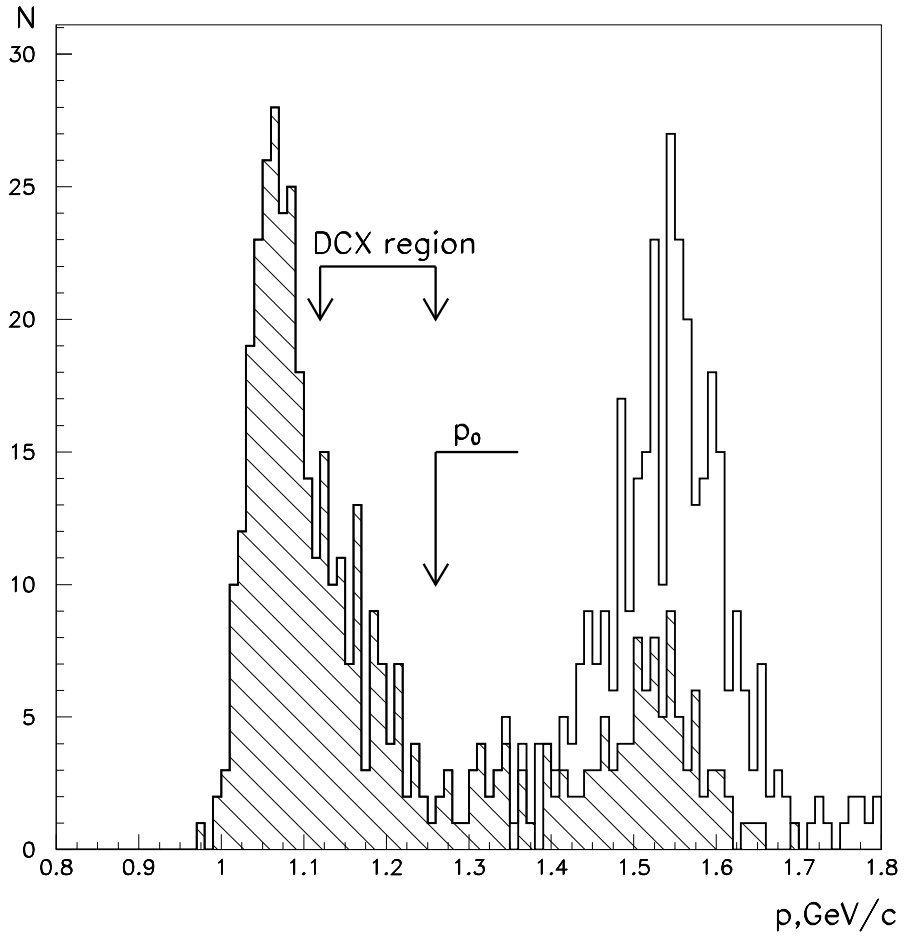

Fig. 5. The momentum distributions of the outgoing particles in the S'_π trigger at T_0 = 1.1 GeV after the cut $|\Delta\lambda| \geq 0.03$ rad to reject beam positron background. The hatched histogram is after the cut on M_t^2 to reject protons. p_0 is the beam momentum.

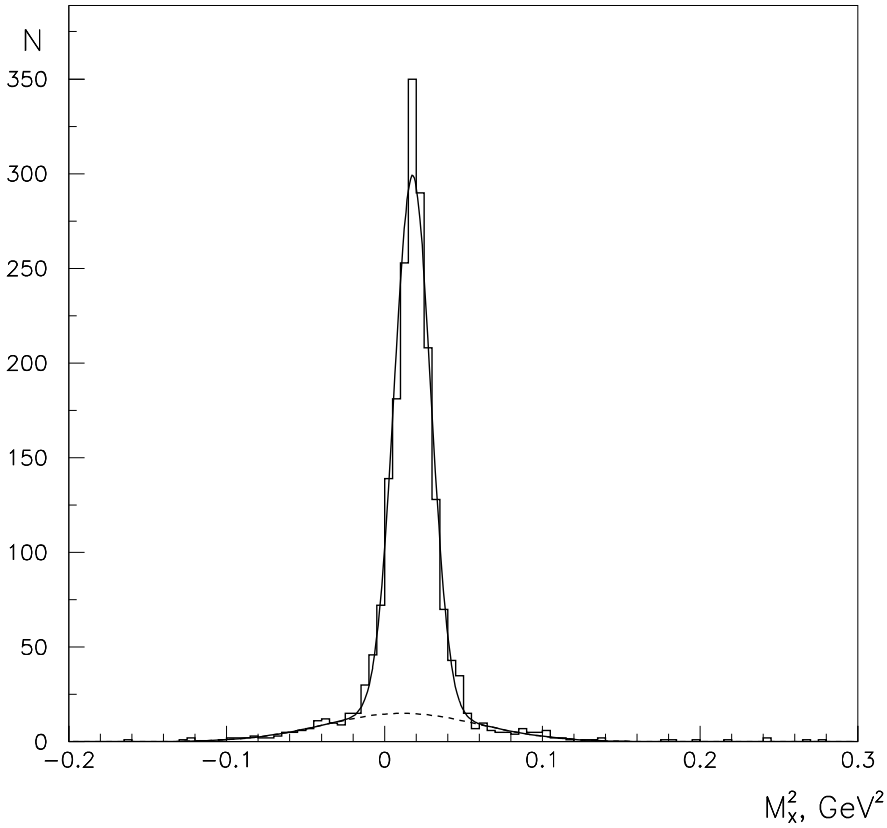

Fig. 6. Missing mass squared for the reaction $\pi^- \mathrm{p} \rightarrow \mathrm{pX}$ on the H_2O target. The solid curve is a two-Gaussian fit with σ = 0.011 and 0.049, and peak positions of 0.018 and 0.011 GeV^2 respectively. The narrower Gaussian describes the elastic (pion) peak while the other, shown by the dashed curve, stands for the oxygen background.

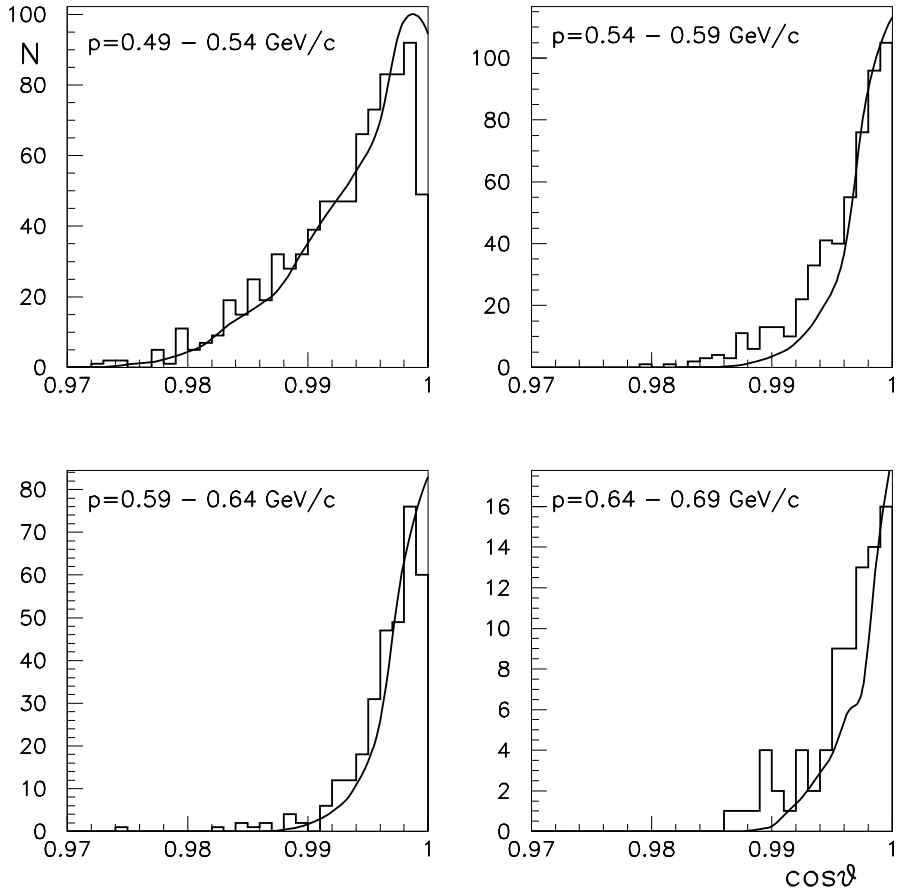

Fig. 7. Angular distributions of events in the reaction (1) for various ranges of the outgoing positive pion momenta. Solid curves represent the acceptance of the apparatus according to the MC calculations assuming a uniform distribution of the cross section on cosθ (arbitrary units).

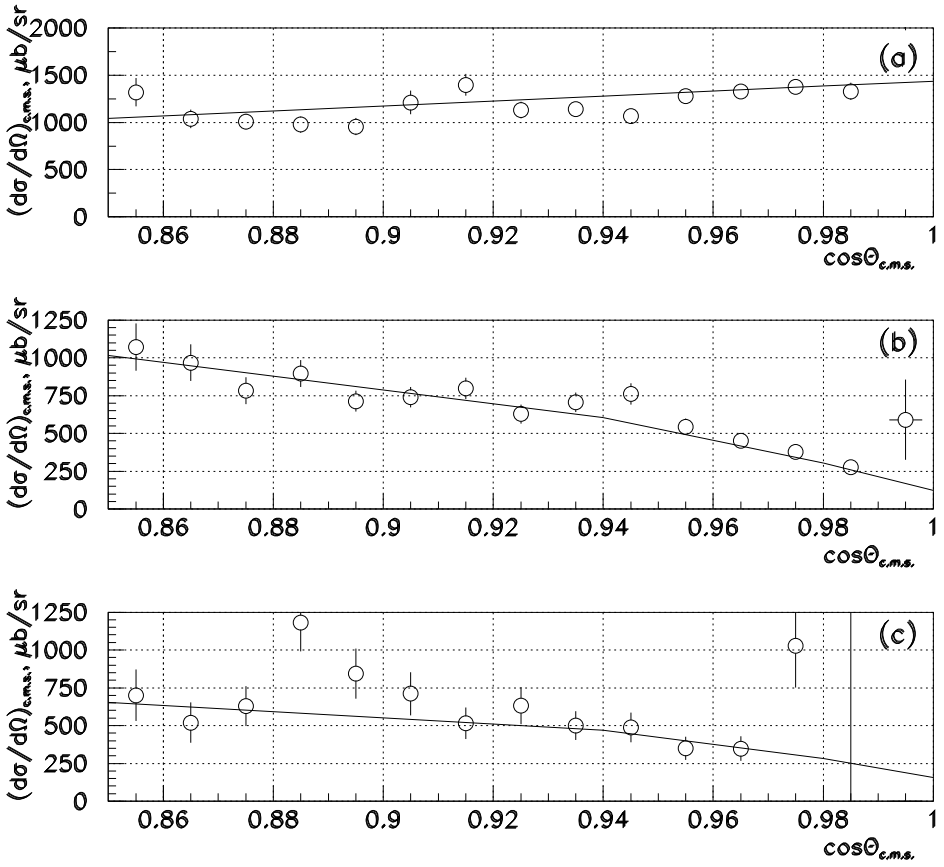

Fig. 8. The differential cross section for the backward $\pi^- \mathrm{p}$ elastic scattering as a function $\cos\theta_{c.m.s}$ ($\theta_{c.m.s}$ is a c.m.s. angle between the incoming pion and the outgoing proton) at $T_0 = 0.59$ GeV (a), $T_0 = 0.75$ GeV (b) and $T_0 = 1.1$ GeV (c). The solid lines are the PWA predictions taken from SAID (FA02 solution). The errors are statistical only.

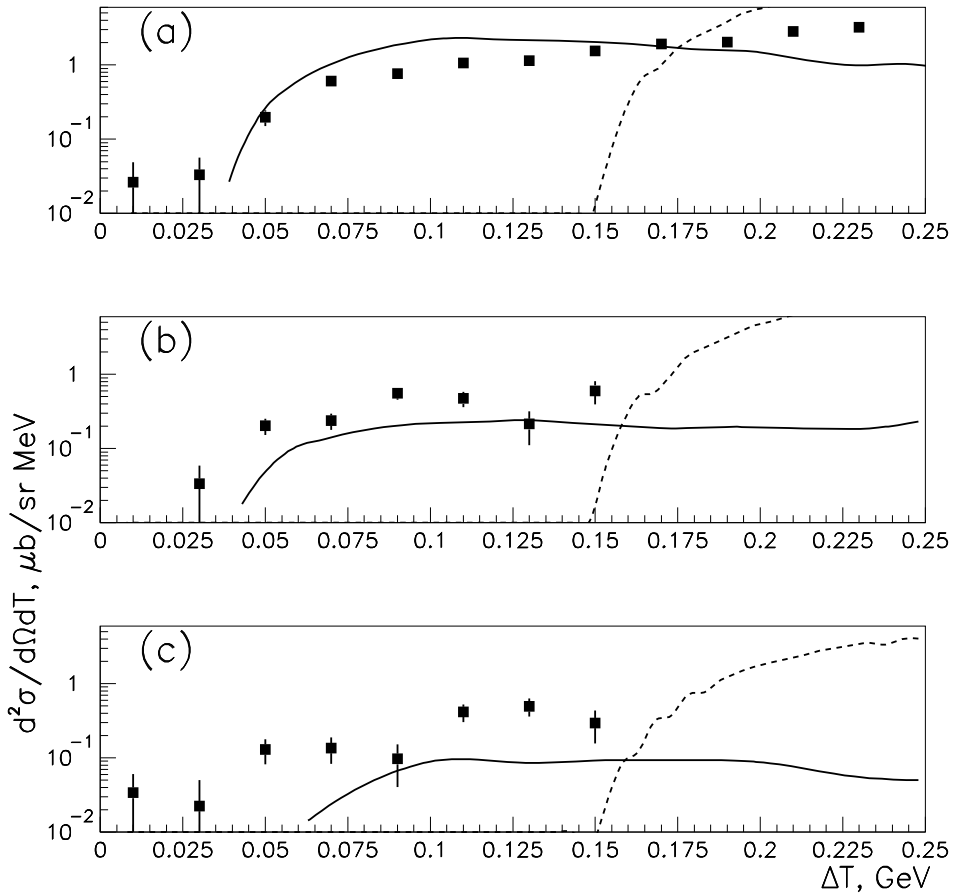

Fig. 9. Differential cross section of the reaction $\pi^{-16}\mathrm{O} \rightarrow \pi^{+}\mathrm{X}$ at $\langle\theta\rangle \approx 5^{o}$ as a function of $\Delta T = T_0 - T$ for different pion beam momenta : (a) T_0 = 0.59 GeV, measured with the S_π trigger; (b) T_0 = 0.75 GeV, sum of both the S_π and the S'_π triggers; (c) T_0 = 1.1 GeV, sum of both the S_π and the S'_π triggers. The solid and dashed curves were calculated in the framework of the MC cascade model for the sequential mechanism (SSCX) and the additional pion production, respectively.

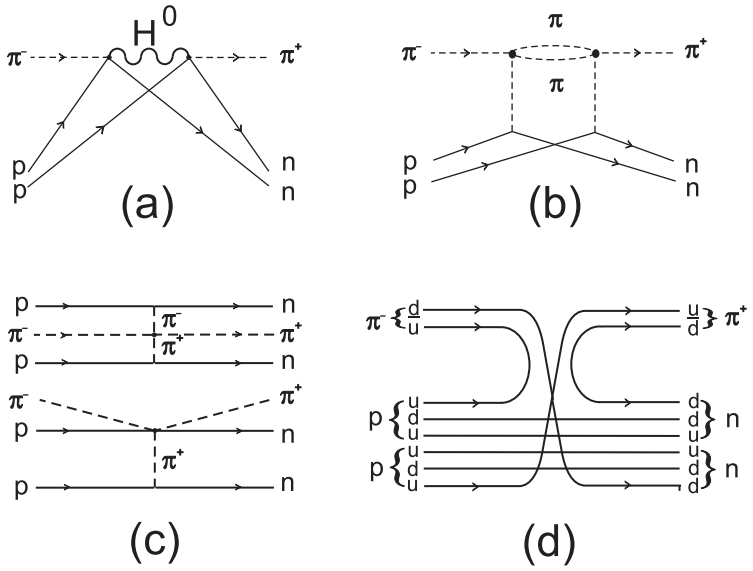

Fig. 10. Diagrams contributing to pion double charge exchange on a nucleus –
(a) sequential charge exchanges on two different protons:
$H^0 = \pi^0$, sequential single charge exchanges (SSCX),
$H^0 = \eta^0, \rho^0 ...$ quasielastic rescatterings,
$H^0 = n\pi$, inelastic Glauber rescatterings ($H^0 = 2\pi^0, \pi^+\pi^-, ...$),
(b) inelastic rescatterings with $H^0 = 2\pi$ in the OPE model,
(c) meson exchange currents (MEC),
(d) short-range NN correlations.

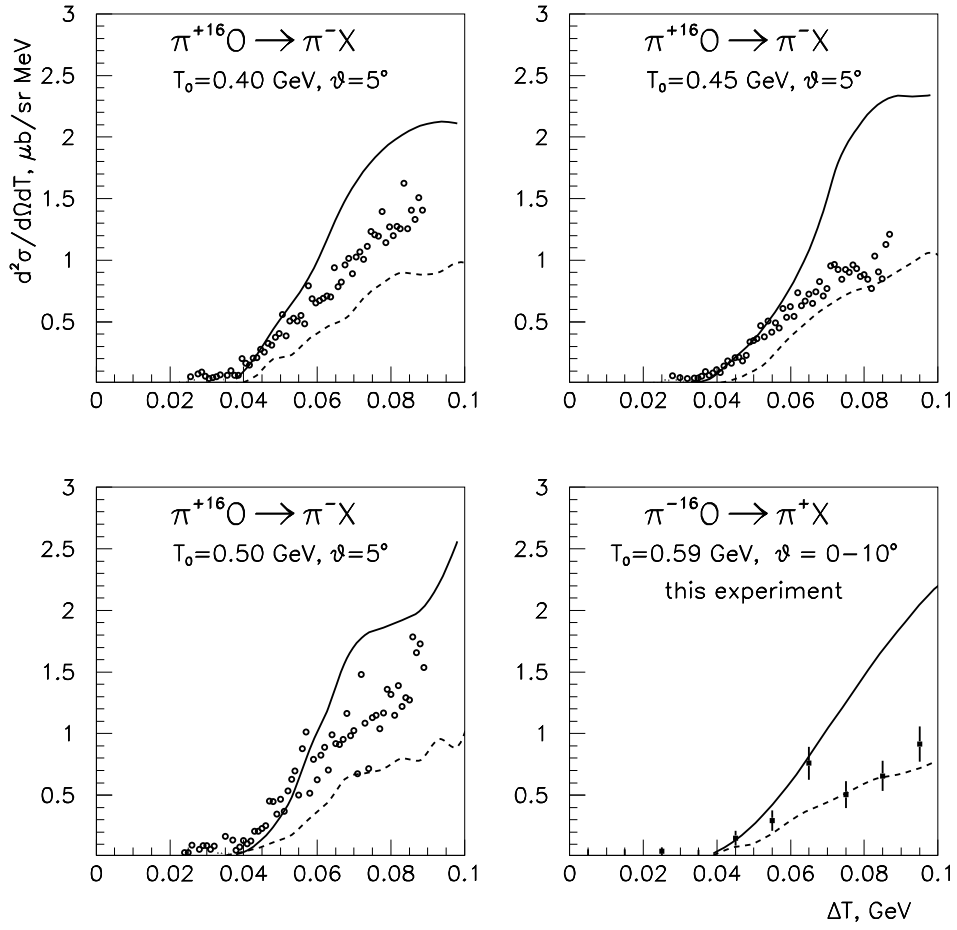

Fig. 11. Double-differential cross sections for $\pi^{+16}\mathrm{O} \to \pi^-\mathrm{X}$ [29] and $\pi^{-16}\mathrm{O} \to \pi^+\mathrm{X}$ reactions versus ΔT. Curves are calculated in the framework of SSCX mechanism with (dashed curve) and without (solid curve) medium polarization.

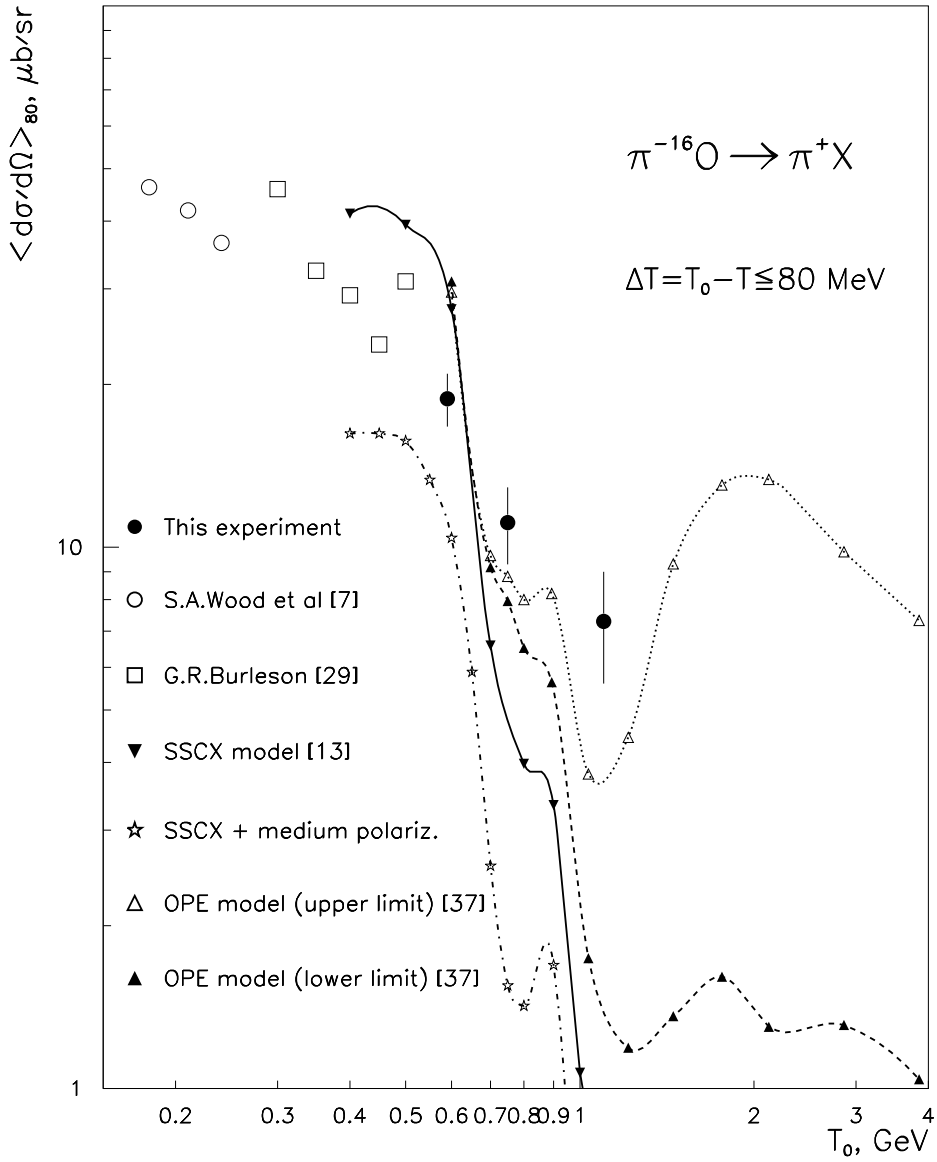

Fig. 12. Energy dependence of the DCX cross section integrated over the ΔT range from 0 to 80 MeV.

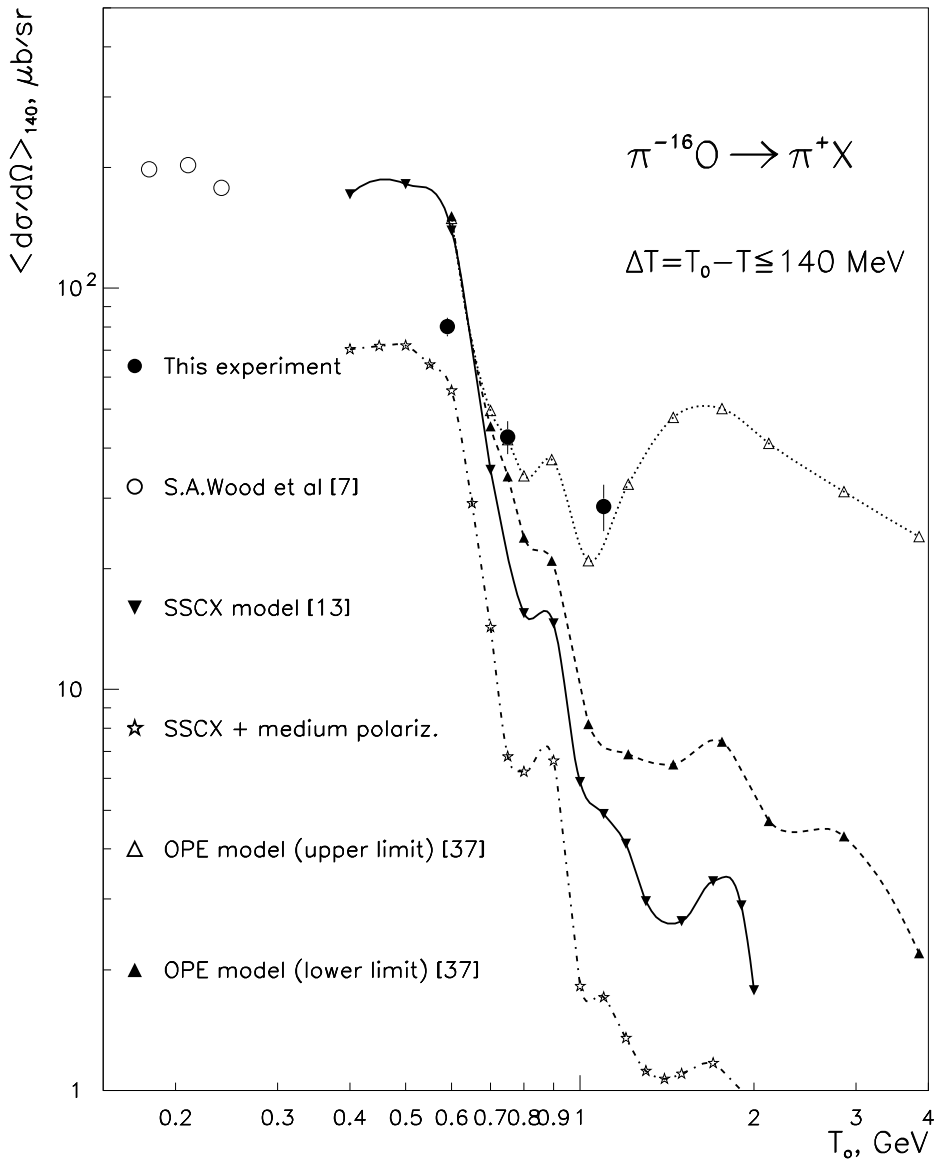

Fig. 13. Energy dependence of the DCX cross section integrated over the ΔT range from 0 to 140 MeV.